Synthesis and Electrocatalytic Performance of NiO Modified Co$_3$O$_4$ Composites for Zinc-Air Batteries

Guanghua Li, Mohammed Adnan Mezaal, Ke Zhang, Lixu Lei[*]

School of Chemistry and Chemical Engineering, Southeast University, Nanjing 211189, China
[*]E-mail: lixu.lei@seu.edu.cn

A series of NiO modified Co$_3$O$_4$ composites were synthesized by the citrate method. The optimal composite is of the Co/Ni atomic ratio of 9:1. The maximum power density achieved by zinc-air battery using this composite is 100.1 mW cm^{-2} at the current density of 148.3 mA cm^{-2}. The zinc-air batteries have discharge capacities 493.0 and 579.5 mAh g^{-1} with the composite with the Co/Ni atomic ratio of 9:1 as catalyst at a constant current density of 30 and 50 mA cm^{-2}, respectively.

1. INTRODUCTION

The concept of sustainability and low-carbon economy urge the people trend to use renewable energy and develop electrical vehicles (EVs) [1]. Recently, zinc-air batteries (ZABs) have caused increasing attention due to their environmentally benign, high specific energy and low operation risks [2]. However, their weak durability, high cost, and sluggish oxygen reduction reaction (ORR) stop their large-scale commercial applications [3]. Thus, ZABs have promoted the development of air electrode on optimizing of new non-noble metal catalyst.

Transition metal oxides such as perovskites [4-6], pyrochlores [7, 8], spinels [9, 10], individual oxides [11], and their mixtures [12, 13] could be used to improve the performance of ZABs. Especially, Co/Co-based oxides and its doped [14-19] were developed to achieve the aim of low cost and high catalytic active materials for the ORR. Such as, the RRDE data show that that the Co$_3$O$_4$ catalyst directs the ORR toward the two-electron pathway [20]. The meso-Co$_3$O$_4$ materials showed a high activity for ORR in 0.1 M KOH solution using rotating disk electrode (RDE) technique[21]. The electrochemical measurements show that the Co$_3$O$_4$ material has better active properties toward the

ORR [22]. The Co_3O_4/C composites with a Co loading content of 4.3 at% showed the best activity for ORR [23]. The discharge performance of Co_3O_4 nanodisks as efficient ORR catalyst is highlighted than commercial Pt/C catalyst for zinc–air battery application [24]. Doping the Co_3O_4/Co_2MnO_4 nanoparticles displayed excellent activities for ORR and OER in alkaline medium [25]. MnO_x modified Co_3O_4/C exhibited better activity for ORR than Co_3O_4/C and MnO_x [26]. The Ni-modified Mn_yO_x resulted in an increased ORR stability [27]. Similarly, Ag modified Co_3O_4 displays a high ORR performance [28]. On the NiO catalyst ORR proceed via two-electron pathway with formation of OH^- ion [29]. In addition, the NiO has better ORR performance in alkaline and acid solutions [30, 31]. In this work, we hence anticipate that the combination of NiO and Co_3O_4 could lead to the production of electrocatalyst with low cost and high activity toward ORR. It can be widely used in the ZABs. Moreover, in order to examine the practical application of NiO/Co_3O_4 catalyst, we measure in the homemade electrochemical cell instead of on the rotating disk electrode (RDE) and rotating ring disk electrode (RRDE) (At present, there are a lot of such data.). So, we hope to provide some practical data in ZABs for others.

2. EXPERIMENTAL

2.1 Synthesis of NiO/Co₃O₄

NiO modified Co_3O_4 hybrid material was prepared by the citrate method [32]. $Co(NO_3)_2 \cdot 6H_2O$, $Ni(NO_3)_2 \cdot 6H_2O$, and citric acid were used as raw materials. The dosage of $Ni(NO_3)_2 \cdot 6H_2O$ changed according to the Co/Ni atomic ratio of 3:2, 7:3, 4:1, 1:9 and 1:0.

2.2 Physical characterization

The material morphology was examined using a SEM (Hitachi S-4800), which was companied to an EDS. Powder analysis was performed using an XRD (Bruker D8 GADDS). Co and Ni contents included in the materials were determined using an ICP (Optima 8000). Thermogravimetric (TG) measurements were carried out by a TA-SDTQ600 thermal analyzer with an air flow at a rate of 10 °C from 50 °C to 900 °C.

2.3 Preparation of air electrode

The air electrode consisted of an active layer, a Ni-mesh current collector and a gas diffusion layer. In the active layer, a mixture containing Co_3O_4 and NiO/Co_3O_4 hybrid materials and acetylene black was grinded for 20 min. Then the mixture and PTFE suspension (60 wt% in H_2O) with weight ratios of 8:2 were mixed and grind in excess ethanol and then dried at 80 °C to give a dough like paste, which was rolled into an Ni-mesh of about 1.8 mm thickness. In order to prevent water seeping from the air electrode, we attached a waterproof layer (polytetrafluoroethylene (PTFE) membrane, only 0.1 mm thick) to the other side of the active layer as a gas diffusion layer.

2.4 Electrochemical characterization

The polarization curves were measured with a half-cell by an electrochemical workstation system (CorrTest CS350). The electrolyte was 7 M KOH solution. The air electrode was used as the working electrode, and an Hg/HgO electrode and a nickel sheet were used for a reference electrode and a counter electrode, respectively.

2.5 Zinc-air battery fabrication and testing

A homemade electrochemical cell was designed for the zinc-air battery test. The electrolyte used in ZABs was 7 M KOH, and a polished Zn sheet was used as the anode. ZABs testing were carried out at 25 °C with a multichannel battery cycling unit (SZLAND CT2001C).

3. RESULTS AND DISCUSSION

3.1 Physical characterization of NiO/Co$_3$O$_4$

To understand the decomposition behaviors of NiO/Co$_3$O$_4$ precursor, the TG curves of the NiO/Co$_3$O$_4$ precursor with Co/Ni ratio of 4:1 is given in Fig. 1. The TGA curve mainly includes two steps of weight loss in Fig. 1. The first step (from 50 to 200 °C) manifests a slight weight loss, which attribute to the evaporation of free water and crystal water. The second step (from 200 to 500 °C) indicates a steep decrease with large weight loss (65.5%), manifesting that the water and the oxynitride of decomposition and the carbon dioxide of formation have totally run out from the precursor. And, after 500 °C, the curve has no obvious weight loss process. It indicates that the Ni/Co citrate be completely converted to NiO/Co$_3$O$_4$ composite.
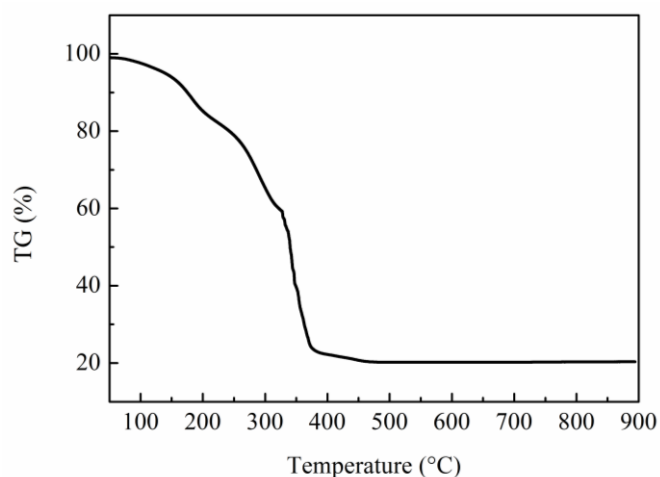

Figure 1. TGA curve of NiO/Co$_3$O$_4$ precursor with Co/Ni ratio of 4:1

XRD patterns for the series of NiO modified Co_3O_4 composites with different Co/Ni atomic ratios are shown in Fig. 2. For comparison, the pattern of Co_3O_4 (JCPDS No. 42-1467) is included in the bottom of Fig. 2. Firstly, it can be observed that the XRD patterns for the composites with the Co/Ni atomic ratio of 9:1, 4:1, 7:3 and 3:2 are comparable and the main phases is Co_3O_4 and NiO. With the with Co/Ni atomic ratio further decreasing, the peaks located at about 43.5°, 50.7° and 74.6° attributed to the NiO in the composites become more and more obvious.
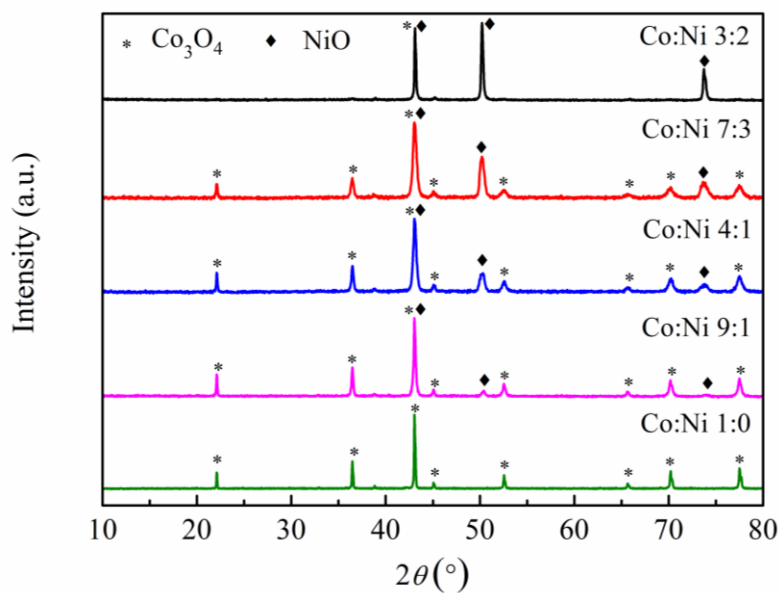

Figure 2. XRD patterns for the NiO modified Co_3O_4 composites with different Co/Ni atomic ratios.
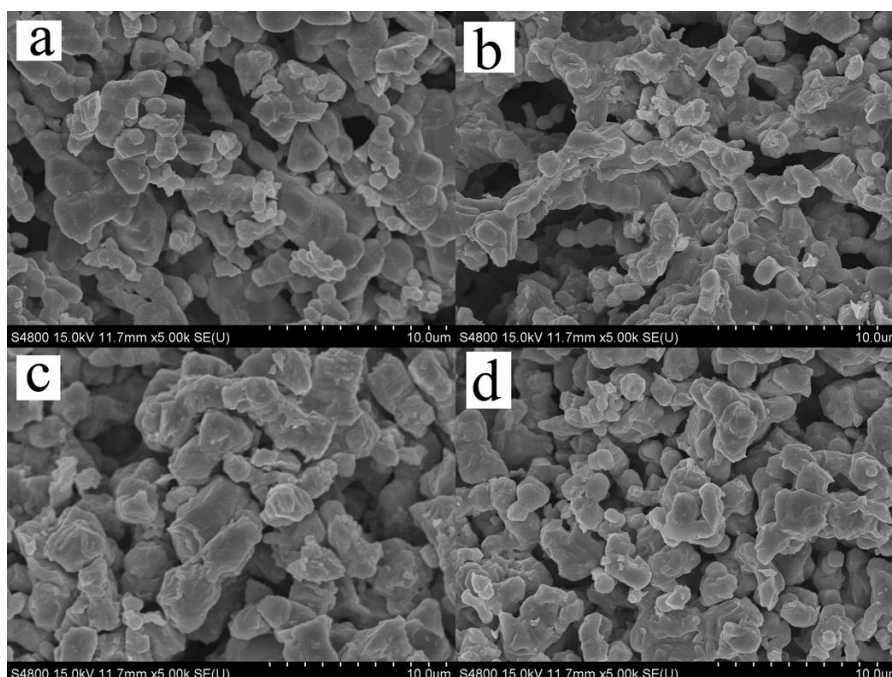

Figure 3. SEM images of NiO/Co_3O_4 hybrid materials with the Co/Ni atomic ratio of 3:2 (a), 7:3 (b), 4:1 (c) and 9:1 (d).

Fig. 3 shows the SEM images of the NiO modified Co_3O_4 composites with the Co/Ni atomic ratio of 3:2 (a), 7:3 (b), 4:1 (c) and 9:1 (d), illustrates the irregular shapes of these particles in an aggregated form with an average diameter of 1 ~ 4 μm. To investigate the composition of the NiO/Co_3O_4, EDS were also carried out (Fig.4). The EDS results confirmed the existence of cobalt and nickel with different proportions (Table 1).
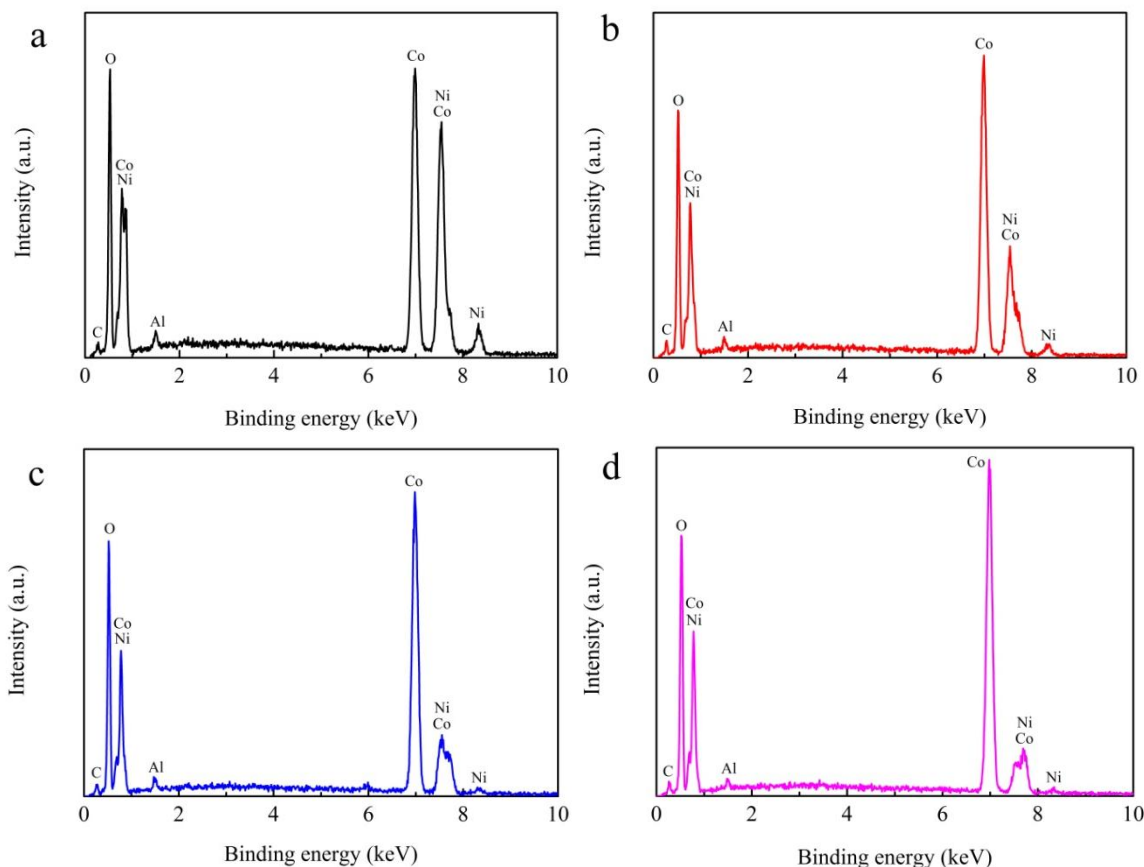

Figure 4. EDS patterns of NiO/Co_3O_4 hybrid materials with the Co/Ni atomic ratio of 3:2 (a), 7:3 (b), 4:1 (c) and 9:1 (d).

Table 1. Atom% of NiO/Co_3O_4 hybrid materials with the different Co/Ni atomic ratio of 3:2, 7:3, 4:1 and 9:1, respectively.

Atom%	O-K	Co-K	Ni-K
Co:Ni 3:2	38.63	31.79	29.58
Co:Ni 7:3	42.98	41.18	15.84
Co:Ni 4:1	44.97	45.97	9.06
Co:Ni 9:1	45.02	49.73	5.26

Co and Ni contents of the materials were determined by ICP. The analytical results are shown in Table 2. It is found that the chemical formula of the prepared samples is $Co_{0.59}Ni_{0.41}$, $Co_{0.70}Ni_{0.30}$,

$Co_{0.78}Ni_{0.22}$, and $Co_{0.89}Ni_{0.11}$, respectively, and is very close to the anticipated $Co_{0.60}Ni_{0.40}$, $Co_{0.70}Ni_{0.30}$, $Co_{0.80}Ni_{0.20}$, and $Co_{0.90}Ni_{0.10}$ chemical stoichiometry, respectively.

Table 2. Element content of the Co/Ni atomic ratio of 3:2, 7:3, 4:1 and 9:1

Sample	$Co_{0.59}Ni_{0.41}$	$Co_{0.70}Ni_{0.30}$	$Co_{0.78}Ni_{0.22}$	$Co_{0.89}Ni_{0.11}$
Co (mg/g)	197	33.8	19.7	2.82
Ni (mg/g)	136	14.4	5.53	0.35

3.2 Electrocatalytic ORR

Fig. 5 shows the cathodic polarization curves for the composites with the Co/Ni atomic ratios of 3:2, 7:3, 4:1, 9:1 and 1:0. As it can be seen, the current density is about 34.1, 44.2, 51.1, 82.7 and 57.3 for ORR at −0.40 V (vs. Hg/HgO 7 M KOH), respectively. At the same potential, the current density increases as the Co/Ni atomic ratio increasing with the maximum value at the Co/Ni atomic ratio of 9:1. Further increasing the Co/Ni atomic ratio makes the current density decrease. It was apparently indicated that the Co/Ni atomic ratio of 9:1 is superior with the highest ORR performance. It was found that the ORR property of the different Co/Ni atomic ratio decreased in the order 9:1 > 1:0 > 4:1 > 7:3 > 3:2. The rodlike Co_3O_4 showed around 96 mA cm^{-2} current density in the same conditions by Kong [22]. Compared with this, the performance has slightly decreased, but the cost down a lot.
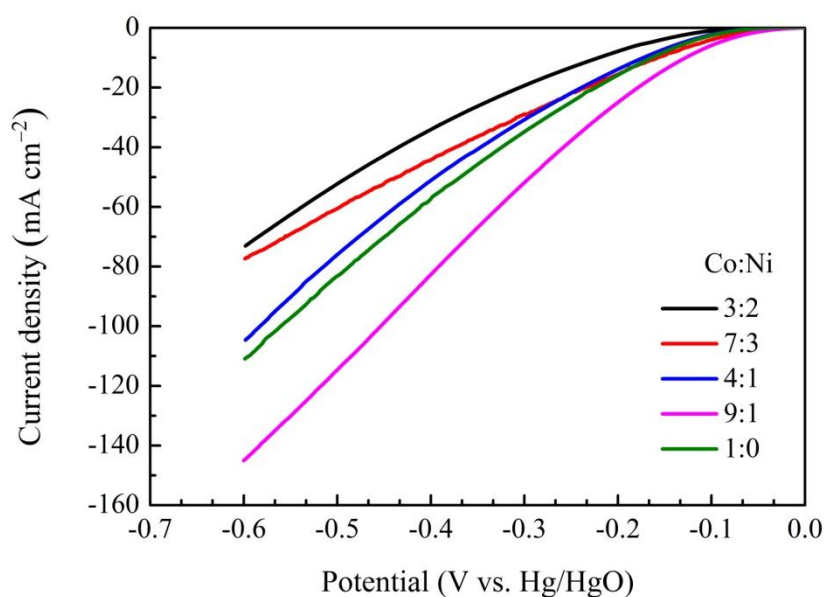

Figure 5. ORR polarization curves of the air electrodes with Co/Ni atomic ratio of 3:2, 7:3, 4:1, 9:1 and 1:0.

3.3 Zinc-air batteries Tests

As discussed before, the NiO modified NiO/Co_3O_4 composite with the Co/Ni atomic ratio of 9:1 has the highest ORR activity. Fig. 6 shows the power density and polarization curves for the composites with the Co/Ni atomic ratios of 3:2, 7:3, 4:1, 9:1 and 1:0. The cells had an open circuit voltage of ∼ 1.40 V. At 1.0 V, the composites with the Co/Ni atomic ratios of 3:2, 7:3, 4:1, 9:1 and 1:0 afforded an ORR current density of 56.1, 61.4, 78.4, 71.8 and 73.6 mA cm^{-2}, respectively. The maximum power density accomplished by zinc-air battery using the composite with the Co/Ni atomic ratio of 9:1 is 100.1 mW cm^{-2} at the current density of 148.3 mA cm^{-2}, which is about 70%, 40%, 10% and 9% higher than that of zinc-air battery using the composite with the Co/Ni atomic ratio of 3:2 (59.0 mW cm^{-2} at 65.1 mA cm^{-2}), 7:3 (71.3 mW cm^{-2} at 93.3 mA cm^{-2}), 4:1 (91.0 mW cm^{-2} at 110.4 mA cm^{-2}) and 1:0 (91.9 mW cm^{-2} at 119.3 mA cm^{-2}), respectively. Similarly, the open circuit voltage of the electrochemical cell with hybrid catalyst MnO_x-Co_3O_4/C was around 1.39 V. At 1.0 V, the current density was around 90 mA cm^{-2} and maximum power density was 97 mW cm^{-2} at 100 mA cm^{-2}. [26]. The current density of the Co_3O_4 nanodisks and commercial 20 wt.% Pt/C catalyst at 1.0 V vs Zn was about 27 mA cm^{-2} [24]. The current density at 1.0 V and the maximum power density of XC72/α-MnO_2 was 40 mA cm^{-2} and 68 mW cm^{-2} at 107 mA cm^{-2} [33]. At 100 mA cm^{-2}, the voltages of the ZABs with MnO_x/C, Ni modified MnO_x/C composite, Pd/C, and Pt/C was 0.83, 0.96, 0.91, and 0.94 V, respectively [13]. This indicates that the doping achieve the ideal effect, can be applied to the zinc air battery.
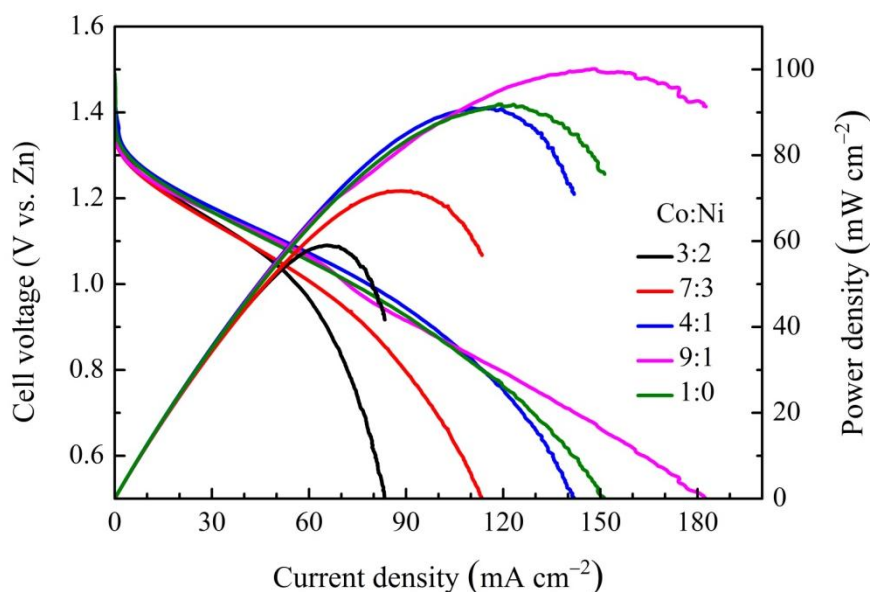

Figure 6. Polarization and power density curves for zinc-air batteries with Co/Ni atomic ratio of 3:2, 7:3, 4:1, 9:1 and 1:0.

Fig. 7 shows the typical discharge profiles of homemade zinc-air cells made with the composites with the Co/Ni atomic ratios of 3:2, 7:3, 4:1, 9:1 and 1:0. At a constant current density of

30 mA cm^{-2} for the cells, the working voltage plateaus were 1.03, 1.03, 1.01, 1.04 and 1.01, respectively. The corresponding specific discharge capacity was found to be 410.8, 422.8, 457.0, 493.0 and 485.2 mAh g^{-1}, respectively. The ZAB with the air cathode containing XC72/α-MnO_2 catalyst exhibited the specific capacity (800 mAh g^{-1}, at 2 mA cm^{-2}) [33]. The results demonstrate that the composite with the Co/Ni atomic ratio of 9:1 is ideally suited for such refueling ZABs due to the exceptional ORR performance and durability.
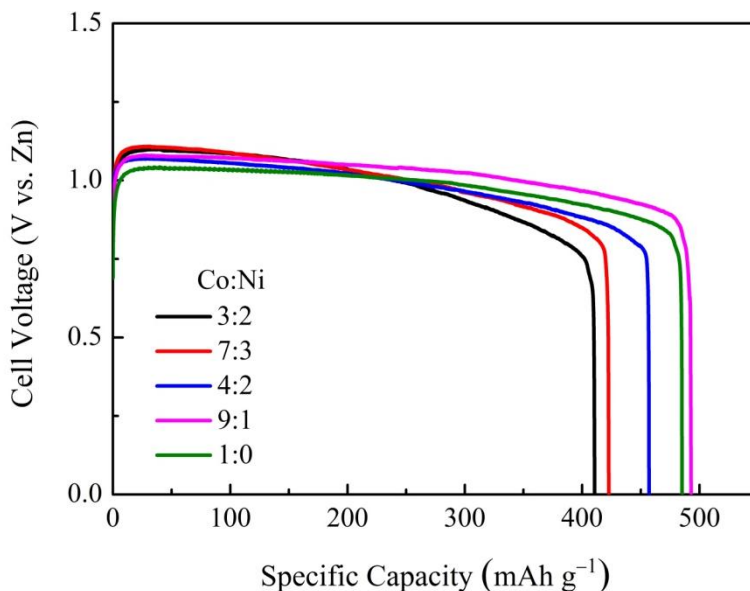

Figure 7. Discharge curves of zinc-air batteries with Co/Ni atomic ratio of 3:2, 7:3, 4:1, 9:1 and 1:0 (At a constant current density of 30 mA cm^{-2}).
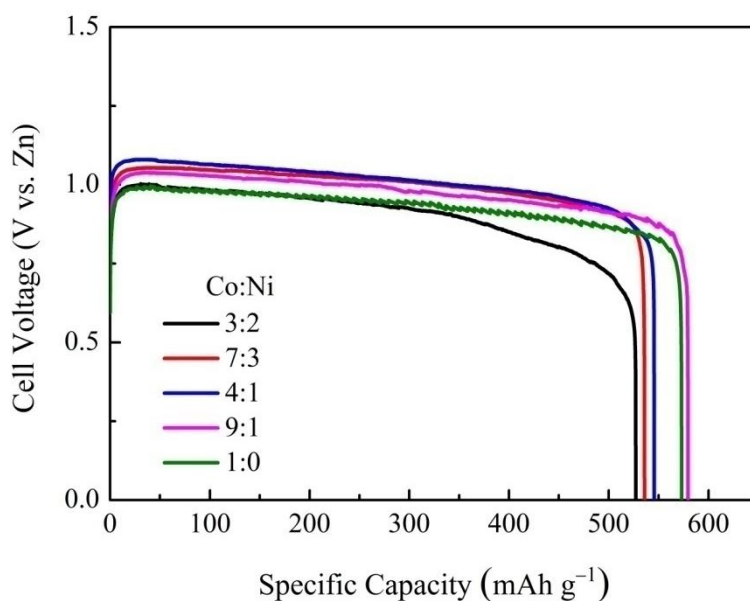

Figure 8. Discharge curves of zinc-air batteries with Co/Ni atomic ratio of 3:2, 7:3, 4:1, 9:1 and 1:0 (At a constant current density of 50 mA cm^{-2}).

Fig. 8 displays the typical discharge profiles of homemade zinc-air cells made with the composites with the Co/Ni atomic ratios of 3:2, 7:3, 4:1, 9:1 and 1:0. At a constant current density of 50 mA cm^{-2} for the cells with the catalysts, the working voltage plateaus were 0.94, 1.02, 1.02, 0.98 and 0.94, respectively. The corresponding specific discharge capacity was also found to be 527.2, 535.8, 545.6, 579.5 and 573.1 mAh g^{-1}, respectively. The specific discharge capacity of cell with the EMD and as-prepared MnO_2 at 50 mA cm^{-2} was 91.7 and 222 mAh g^{-1}, respectively [34]. The results also indicate that the composite with the Co/Ni atomic ratio of 9:1 is ideally suited for such refueling ZABs.

4. CONCLUSIONS

For the series of NiO modified Co_3O_4 composites with varied Co/Ni atomic ratios, prepared by a citrate method. The higher activity of the composites toward the ORR is related to the Co/Ni atomic ratios. The electrochemical tests show that the composite with the Co/Ni atomic ratio of 9:1 has the best ORR activity. With the optimized NiO modified Co_3O_4 composite as the cathode catalyst, the peak power density of the zinc-air battery reaches 100.1 mW cm^{-2} at the current density of 148.3 mA cm^{-2}. The zinc-air batteries have discharge capacities 493.0 and 579.5 mAh g^{-1} with the composite with the Co/Ni atomic ratio of 9:1 as catalyst at a constant current density of 30 and 50 mA cm^{-2}, respectively. Although the performance have not remarkable improved, the cost down a lot. In the future, the ZABs using this catalyst will be used widely in daily life.

References

1. M. Armand, J.-M. Tarascon, *Nature* 451 (2008) 652-657.
2. Y. Li, H. Dai, *Chemical Society reviews* 43 (2014) 5257-5275.
3. R. Cao, J.-S. Lee, M. Liu, J. Cho, *Advanced Energy Materials* 2 (2012) 816-829.
4. W. Zhou, J. Sunarso, *The Journal of Physical Chemistry Letters* 4 (2013) 2982-2988.
5. J. Hu, L. Wang, L. Shi, H. Huang, *Journal of Power Sources* 269 (2014) 144-151.
6. D.U. Lee, H.W. Park, M.G. Park, V. Ismayilov, Z. Chen, *ACS applied materials & interfaces* 7 (2015) 902-910.
7. S. Malkhandi, P. Trinh, A.K. Manohar, K.C. Jayachandrababu, A. Kindler, G.K. Surya Prakash, S.R. Narayanan, *Journal of the Electrochemical Society* 160 (2013) F943-F952.
8. S.H. Oh, R. Black, E. Pomerantseva, J.-H. Lee, L.F. Nazar, *Nature chemistry* 4 (2012) 1004-1010.
9. Y. Liang, H. Wang, J. Zhou, Y. Li, J. Wang, T. Regier, H. Dai, *Journal of the American Chemical Society* 134 (2012) 3517-3523.
10. X. Ge, Y. Liu, F.W. Goh, T.S. Hor, Y. Zong, P. Xiao, Z. Zhang, S.H. Lim, B. Li, X. Wang, Z. Liu, *ACS applied materials & interfaces* 6 (2014) 12684-12691.
11. Y.J. Huang, Y.L. Lin, W.S. Li, *Electrochim. Acta* 99 (2013) 161-165.

12. G. Du, X. Liu, Y. Zong, T.S. Hor, A. Yu, Z. Liu, *Nanoscale* 5 (2013) 4657-4661.
13. Q. Wu, L. Jiang, L. Qi, E. Wang, G. Sun, *International Journal of Hydrogen Energy* 39 (2014) 3423-3432.
14. X.G. Fu, J.T. Jin, Y.R. Liu, Q. Liu, K.X. Niu, J.Y. Zhang, X.P. Cao, *Electrochemistry Communications* 28 (2013) 5-8.
15. J. Xiao, Q. Kuang, S. Yang, F. Xiao, S. Wang, L. Guo, *Scientific reports* 3 (2013) 2300.
16. J. Wu, D. Zhang, Y. Wang, Y. Wan, B. Hou, *Journal of Power Sources* 198 (2012) 122-126.
17. Y. Liang, Y. Li, H. Wang, J. Zhou, J. Wang, T. Regier, H. Dai, *Nature materials* 10 (2011) 780-786.
18. R. Huo, W.J. Jiang, S. Xu, F. Zhang, J.S. Hu, *Nanoscale* 6 (2014) 203-206.
19. M. Hamdani, R.N. Singh, P. Chartier, *International Journal of Electrochemical Science* 5 (2010) 556-577.
20. S. Li, G. Zhu, P. Qiu, G. Rong, M. Pan, *Chinese Journal of Catalysis (Chinese Version)* 32 (2011) 624-629.
21. Y.J. Sa, K. Kwon, J.Y. Cheon, F. Kleitz, S.H. Joo, *Journal of Materials Chemistry A* 1 (2013) 9992.
22. F. Kong, Electrochimica Acta 68 (2012) 198-201.
23. Y. Wang, X. Cui, L. Chen, C. Wei, F. Cui, H. Yao, J. Shi, Y. Li, *Dalton transactions* 43 (2014) 4163-4168.
24. D.U. Lee, J. Scott, H.W. Park, S. Abureden, J.-Y. Choi, Z. Chen, *Electrochemistry Communications* 43 (2014) 109-112.
25. D. Wang, X. Chen, D.G. Evans, W. Yang, *Nanoscale* 5 (2013) 5312-5315.
26. Y. Wang, X. Ma, L. Lu, Y. He, X. Qi, Y. Deng, *International Journal of Hydrogen Energy* 38 (2013) 13611-13616.
27. A.C. Queiroz, F.H.B. Lima, *Journal of Electroanalytical Chemistry* 707 (2013) 142-150.
28. Y. Wang, X. Lu, Y. Liu, Y. Deng, *Electrochemistry Communications* 31 (2013) 108-111.
29. A. Trunov, *Electrochimica Acta* 105 (2013) 506-513.
30. T.Y. Yung, L.Y. Huang, T.Y. Chan, K.S. Wang, T.Y. Liu, P.T. Chen, C.Y. Chao, L.K. Liu, *Nanoscale research letters* 9 (2014) 444.
31. S. Ci, J. Zou, G. Zeng, Q. Peng, S. Luo, Z. Wen, *RSC Advances* 2 (2012) 5185.
32. X. Wang, P.J. Sebastian, M.A. Smit, H. Yang, S.A. Gamboa, *Journal of Power Sources* 124 (2003) 278-284.
33. P.C. Li, C.C. Hu, T.C. Lee, W.S. Chang, T.H. Wang, *Journal of Power Sources* 269 (2014) 88-97.
34. G.Q. Zhang, X.G. Zhang, H.L. Li, *Journal of Solid State Electrochemistry* 10 (2005) 995-1001.